International Journal on Interactive Design and Manufacturing (IJIDeM)
https://doi.org/10.1007/s12008-023-01479-2

ORIGINAL PAPER

Numerical and experimental thermal stress analyses of dissimilar GTA welded joints

Abhishek Saxena[1,2] · Kuldeep K. Saxena[3] · Bharat Singh[1] · S. K. Rajput[4] · Balram Yelamasetti[5]

Received: 19 March 2023 / Accepted: 30 July 2023

Abstract
In this work, temperature profiles and residual stresses were measured experimentally for validating the predicted temperature gradients and thermal stresses developed in dissimilar gas tungsten arc weldments of AA 6082 and AA 7075. The temperature dependent thermo-mechanical properties were considered along with convective and radiation boundary conditions during analysis. SOLID 90 and SOLID 185 elements are chosen for analysis in this research. The predicted thermal fields and stresses were validated experimentally using Infra-Red (IR) Thermography and X-Ray diffraction techniques. The peak temperature is recorded in pass-3 when compared to remaining passes and the lower temperature was recorded near the AA7075 heat affected zone. The predicted thermal fields from finite element analysis are in accordance with measured thermal fields using IR thermography with the deviation of 7.5% only.

Keywords Mg-based Al-alloy · Zn-based Al-alloy · Finite element analysis · Temperature fields-IRT · Residual stress-XRD

1 Introduction

Weld joints developed with fusion welding process are mostly known to have thermal distortions leading to poor dimensional accuracies and inferior mechanical properties. Further, residual stresses are induced with in the joints resulting in fatigue fracture and Stress Corrosion Cracking (SCC) near the welding roots [1, 2]. Weld root defects require special attention in the structures of pressure vessels, petrochemical equipment's, offshore structures which are produced using Gas Tungsten Arc Welding (GATW) process [3, 4]. GTAW has also been a commonly used fusion welding technique for joining high strength materials because of quality welded structures which it produces in all welding positions [5, 6]. During joining of dissimilar metals, suitable welding and filler play a vital role for producing sound welded structures. Dissimilar weldments have always been under discussion because of difficulty in joining them to achieve suitable weld properties than similar weldments because of following differences such as chemical compositions, phase structures and properties of dissimilar metals and filler metals [7–10].

The heat flow during heating and cooling cycles provides the essential characteristics in the welded structures. Thus, to achieve a welded structure of desired specifications to perform satisfactorily in service, it is important to know the peak values of temperatures and their distribution in thermal cycles along longitudinal and transverse directions [11]. Infra-Red Thermography (IRT) is one of the most accurate methods among the Non Destructive Testing (NDT) methods to record surface thermal gradients on base metals during welding process [12]. Karunakaran [13] reported the effect of pulse and Constant Current (CCGTAW) process parameters on temperature maps across weldments of Mg alloys. The temperature measurement was made across the weld line at 5 mm, 15 mm and 30 mm for a duration of 250 s. CCGTAW process has recorded a higher peak temperature of 359 °C as compared to 397 °C in Pulsed Current (PCGTAW) process

✉ Balram Yelamasetti
Balram3072@gmail.com

1 Department of Mechanical Engineering, GLA University, Mathura 281406, India

2 Department of Mechanical Engineering, ABES Engineering College, Ghaziabad 201009, UP, India

3 Division of Research and Development, Lovely Professional University, Phagwara 144411, India

4 Department of Mechanical Engineering, BIET, Jhansi 284001, India

5 Department of Mechanical Engineering, MLR Institute of Technology, Hyderabad, Telangana 500043, India

Published online: 01 September 2023

due to higher cooling rates. Vasudevan et al. [14] used the IRT system in-situ camera for monitoring of the weld pool temperatures in GTAW process. The IR results indicated that the developed 316LN stainless steel weldments have defects such as inclusions, lack of fusion and penetration. Balram et al. [15] adopted IR Thermography for recording the temperature distribution. Higher peak temperatures are recorded in CCGTAW process due to continuous heat input when compared with pulsed current GTAW temperatures. Harinadh et al. [16] used IRT for measuring thermal cycles during and after welding process for the development of dissimilar welds of Inconel and steel 316L. Higher temperature gradients were identified in steel 316L side than the Inconel due to its thermal conductance.

Residual Stresses (RS) are defined as the internal stresses which remains in a material when the loads are removed. The developed stresses must be stationary and self-balanced within the material. Due to these residual stress's weldments, the performance of a welded structures may get reduced during service. Fatigue and crack fractures near weld regions caused by tensile nature of residual stresses while compressive natured residual stresses withstand stress corrosion and vanishing of cracks [17–20]. Javadi et al. [21] focused at sub-surface regions to measure the residual stress developed in AISI 316LN and P91 Ferrite steel along with surface measurement. Although deviations and uncertainties with possible errors were found in all of the above techniques, the same techniques have been suggested to be suitable for surface and sub-surface characterization. Zhou et al. [22] joined the similar welds of high strength steel EH47 using multiple-pass welding. The experimental results have shown that compressive residual stresses (CRS) along the fusion line and its nature changed from CRS to tensile residual stresses (TRS) in the HAZ of EH47 steels. The developed RS were observed experimentally and through FEA. Xia et al. [23] discussed on the effect of weld geometry and base metal thickness on formation of RS.

Gaussian model can be used for plotting temperature gradients and residual stresses within AISI 304L joints [24]. The Gaussian heat source model has given accurate predictions, closer to experiment results, of the thermal gradients and residual stresses for thin plates [25]. Vemanaboina et al. [26] developed Gaussian model for simulating laser welding for plotting temperature gradient curves and residual stress distribution. ANSYS APDL module was used for obtaining simulation results. The combined Gaussian surface heat source and volumetric heat flux together as a heat source along the weld line for predicting the temperature gradients and thermal stresses in welds developed with an arc welding process. The experimentally measured values and large displacement theory predicted distortions were mutually agreeable [27].

For predicting more accurate results, 3-D Goldak moving heat source model is used by writing the codes in APDL (ANSYS Module), which would give simulation results of dissimilar sheets combinations, for laser welding process. The results of FE analysis and experimental data of thermal cycles and induced stresses are in good accord [28, 29]. Chen et al. [5]. Investigated on temperature distribution, residual stresses, and weld distortion are experimentally and numerically and concluded that longitudinal RS distribution induced in the lower region of the plates has a major effect in the weld induced thermal distortion. Yegaie et al. [30] developed a thermo-mechanical analysis of the GTAW process for Monel 400 plates with a heat sink. The obtained results show that due to the heat sink, thermal concentration zones were constrained to the vicinity of the heat source model [16]. Yaohui et al. [31] obtained theoretical values of residual stresses developed in joints of Aluminum alloy sheets. The numerical and experimentation results of thermal stress at the center of fusion zone are very close for validation. Jingwei et al. [32] compared the numerically estimated RS with experimental values of Ni-based super alloy weld joints obtained from GTAW. The compressive natured hoop and radial RS were predicted in weld region [33].

From the literature review, it was identified that many researchers have developed various welding simulation models using ANSYS® software but less studies were reported using APDL codes in ANSYS® workbench. The dissimilar combination of AA6082 and AA7075 weldments have wide range of application in automobile industries, aerospace industries, etc. Development of sound welded structures in aluminum joints using fusion welding process is difficulty challenge [34]. In this investigation, the numeral and experimental analyses are carried out to predict and measure the temperature fields and RS established in dissimilar joint between aforementioned base metals. In order to predict peak temperatures, thermal histories and residual stress distribution in these joints, ANSYS® 19.0 is used. For validating these results obtained from FE analysis, IRT and XRD methods are used to measure the thermal cycles and stresses, respectively.

2 Numerical simulation

The numerical simulation of dissimilar weldments between AA6082 and AA7075 is carried out to observe the temperature distribution. For 3 passes such as root pass, filling pass and capping pass the temperature distribution of each pass at time intervals 10 s, 25 s and 44 s is predicated and followed with structural analysis to predict the RS of the specimens. The consider heat source is double ellipsoidal model in the present analysis. The numerical simulation work followed in this research is shown in Fig. 1.

Table 1 Thermo-mechanical properties of AA6082

Temperature (°C)	Mass Density (kg/m^3)	Thermal expansion (W/m-°C)	Young's modulus (Pa)	Thermal conductivity (W/m-°C)	Specific heat (J/Kg-°C)
10	2781	21×10^{-6}	72×10^9	162	900
80	2756	24×10^{-6}	68×10^9	168	980
180	2695	25×10^{-6}	64×10^9	193	1070
280	2650	26×10^{-6}	56×10^9	206	1100
380	2610	27.5×10^{-6}	40×10^9	225	1150
480	2605	28.5×10^{-6}	22×10^9	237	1200

Table 2 Thermo-mechanical properties of AA7075

Temperature (°C)	Density (kg/m^3)	Thermal expansion (W/m-°C)	Young's modulus (Pa)	Thermal conductivity (W/m-°C)	Specific heat (J/Kg-K)
10	2810	22×10^{-6}	72×10^9	121	862
80	2780	24×10^{-6}	71.5×10^9	131	913
180	2760	25.6×10^{-6}	70×10^9	140	955
280	2740	27.2×10^{-6}	64×10^9	148	994
380	2720	28×10^{-6}	52×10^9	155	1036
480	2696	32×10^{-6}	38×10^9	161	1084

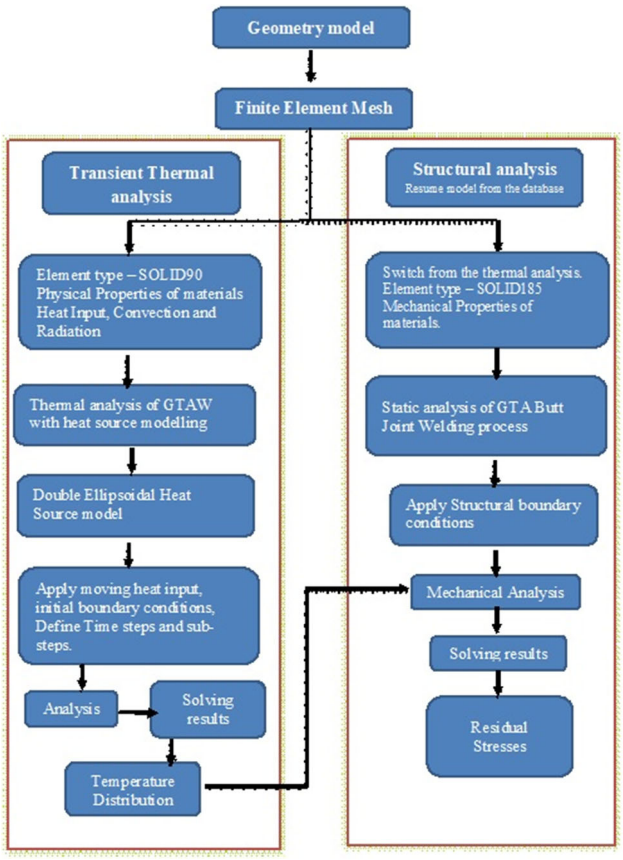

Fig. 1 Methodology of numerical simulation

2.1 FE modeling

The 3-D welding structure of dimensions 150 mm × 100 mm × 5 mm is modelled using CAD software. The structure is modeled with a 1 mm root face and a root gap of 1.5 mm. To differentiate the various zones in the weldment, different meshing zones are generated to predict better results as shown in Fig. 2. For modeling, different type of elements used for thermal and structural analysis (SOLID 90 & SOLID 185 shown in Fig. 3). The temperature dependent properties of both metals are listed in Tables 1 and 2 [34].

2.2 Heat source model

Goldak double ellipsoidal model [35] is implemented as heat source for TIG arc welding in this research. This model has more suitable when the welding current is higher and thick welded structures. The heat is distributed into two parts where high heat is carried out in front quadrant of ellipsoid whereas lower heat is carried out in rear quadrant of ellipsoid (shown in Fig. 4). The welding path, heat input rates and other BC's are mentioned during simulation. For time increments, a modified Newton–Raphson technique (Eq. 1) is chosen (Fig. 4).

$$q(x,\ y,\ z) = \frac{6\sqrt{3} f \eta Q}{abc\pi\sqrt{\pi}} \exp\left(-\frac{3x^2}{a^2} - \frac{3y^2}{b^2} - \frac{3z^2}{c^2}\right) \quad (1)$$

The heat source equation of the quadrant (front) is described as Eq. (2) which will carry the higher heat input

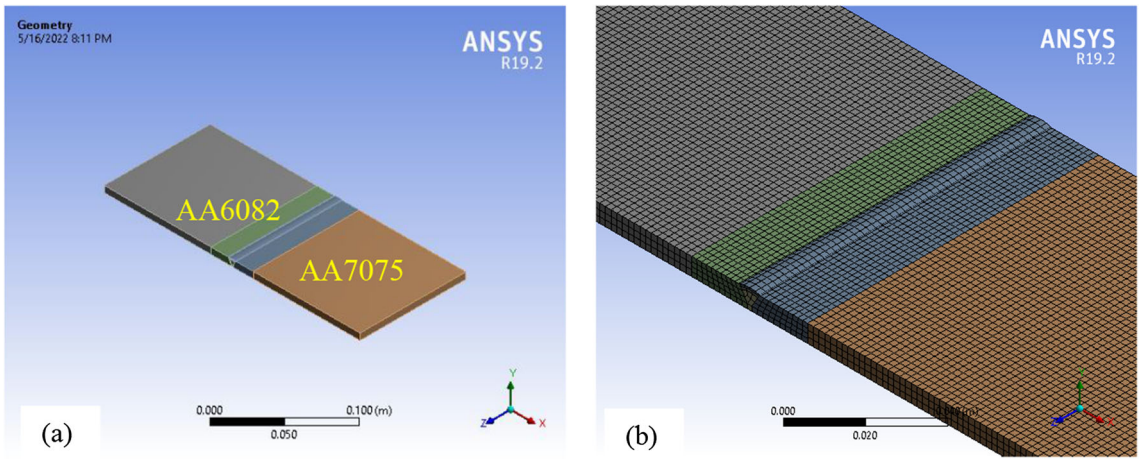

Fig. 2 **a** Welding model of dissimilar weld and **b** fine meshing of model

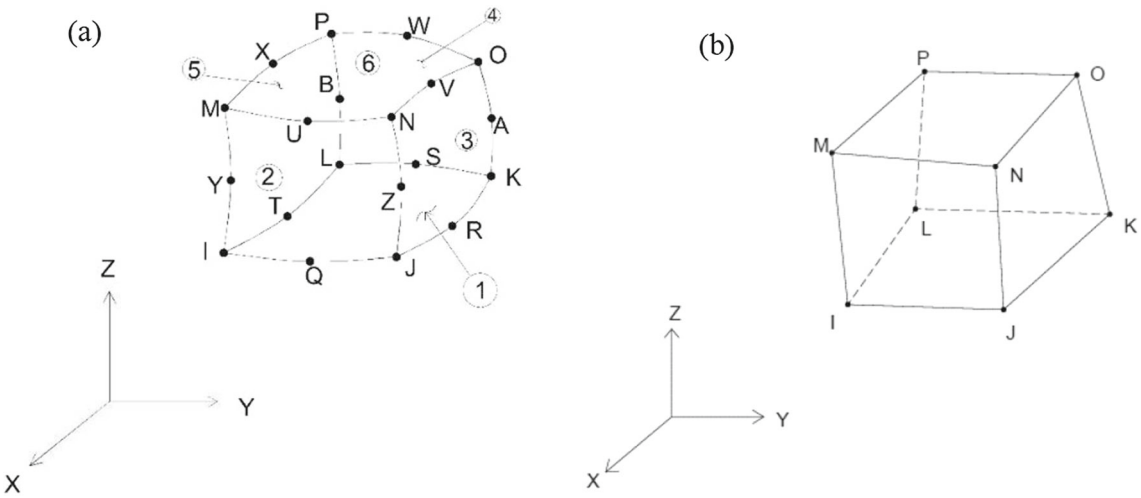

Fig. 3 Elements used in analusisn **a** SOLID 90, **b** SOLID 185

rates.

$$q_f(x,\ y,\ z) = \frac{6\sqrt{3} f_f \eta Q}{abc_f \pi \sqrt{\pi}} \exp\left(-\frac{3x^2}{a^2} - \frac{3y^2}{b^2} - \frac{3z^2}{c_f{}^2}\right) \quad (2)$$

The heat source equation of the quadrant (rear) is described as Eq. (3) which will carry the higher heat input rates.

$$q_r(x,\ y,\ z) = \frac{6\sqrt{3} f_r \eta Q}{abc_r \pi \sqrt{\pi}} \exp\left(-\frac{3x^2}{a^2} - \frac{3y^2}{b^2} - \frac{3z^2}{c_r{}^2}\right) \quad (3)$$

2.3 FE analysis

The boundary condition of thermal study has given on weld plate area as shown in Fig. 5a. From the simulation results it is observed that uneven thermal fields have been generated around the weld line of GTAW process that would result in the formation of RS in welded components. The data of thermal analysis is taken at different time intervals to validate with the recorded temperature profiles. The data predicted from this analysis is used further for structural analysis in order to predict the RS formation in the structures. The fixed and set of boundary conditions are used for better results during analysis. The elastic–plastic analysis was chosen for finding the stresses from thermal histories. Thermal loads from the simulation results are considered as body forces which is equivalent of static analysis as shown in Fig. 5b. The complete research flow of this paper is mentioned in Fig. 6 as a flow chart.

3 Materials and experimental details

The base metals, AA6082 and AA7075, of size 150 × 100 × 5 mm are selected for developing the dissimilar welds

Fig. 4 Heat source model

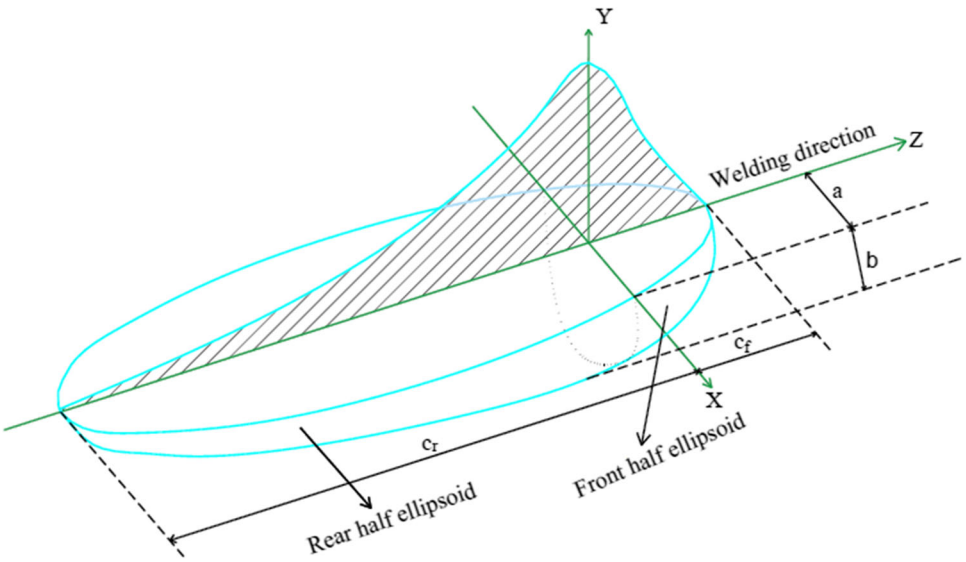

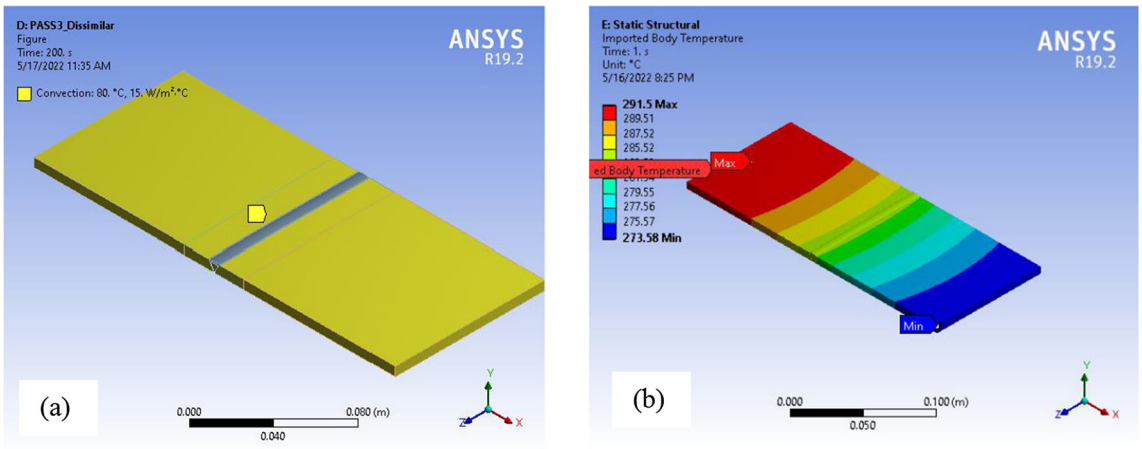

Fig. 5 **a** 3-passes model and **b** convective boundary conditions

Table 3 Composition of alloying elements of base/filler metals [28, 34]

Base/filler metals	Al	Mg	Zn	Cr	Mn	Si	Cu	Fe
AA6082	Bal	1.2	0.09	0.25	0.8	0.8	0.09	0.5
AA7075	Bal	2.8	5.9	0.19	0.02	0.06	1.91	0.14
ER4043	Bal	0.09	0.1	–	0.05	4.58	0.3	0.8

Table 4 Parameters (TIG) used in welding process

Specimen pass no	Weld current, (A)	Voltage drop, (V)	Heat input, Q (W)	Process time, (s)	Torch speed, (mm/s)
Pass1—root pass	185	5.7	1054	46	1.5
Pass2—filling pass	180	5.6	1008	46	2.61
Pass 3—capping pass	180	5.6	1008	45	2.66

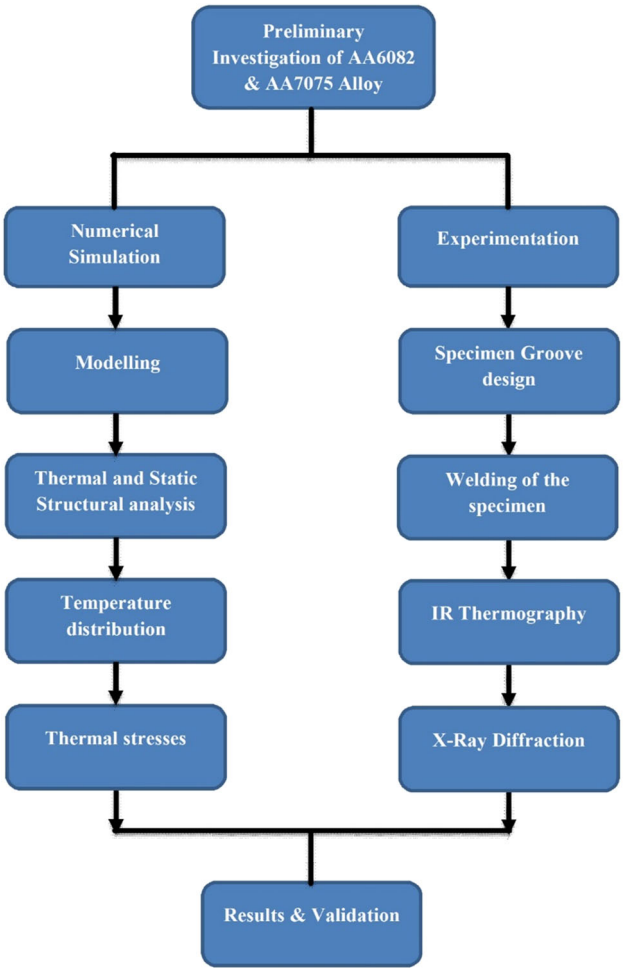

Fig. 6 Flow chart of research work

with multiple passes. GTA welding process was selected for producing root, filling and capping passes welded components using ER4043 as filler rod of 1.6 mm diameter. In this research, LINCOLN 375 welding machine is used. The composition (wt%) of parent metals and filler are listed in Table 3. The GTAW set-up with clamping is shown in Fig. 7. Multi-passes with V-groove shape with same root gap as mentioned in simulation (shown in Fig. 8). The welding parameters adopted from simulation work after number of trails and the optimum values are mentioned in Table 4 for producing the dissimilar joint. Preheating conditions (temperature range 80 to 120 °C) were also maintained in experimental work for capping and filling passes. The developed welded structures and their X-ray radiography film images in three passes as shown in Fig. 9. From, radiography test, the welded structures were free from macro/micro defects and observed uniform weld bead formation throughout the weld line.

3.1 IRT-temperature recording

From the results of IR thermal imager, we analyze the data of three samples of each pass of the weldments. Fluke Ti450 is based on IR-Fusion technology gives an absolute temperature profile with visual details to the infrared images having a measurement range − 20 to 1200 °C with an accuracy of ± 0.1 °C. The Fluke thermal imager captures the images and stores the temperature measurement data of each pass of complete welding across the visual zone of the specimen. By using the SMART VIEW 4.3 software we can visualize the data, captured by the thermal imager. Begin welding, capture of the images is carried out by the thermal imager only after entering the emissivity values of specific material, which are examined. From the literature survey, the emissivity values of AA7075 and AA 6082 has been taken as ε = 0.34. A snapshot of each pass visual data is shown in the below Fig. 10.

3.2 Residual stress

The XRD technique is widely used for calculating stress distribution in the welded structures including sub-surfaces of the components [12]. Due to the uneven thermal behavior of base plates and heating cycles, the lattice structures are get strained internally thus resulting formation of residual stresses. The formation of RS in any welded structures is shown in Fig. 11. The equations used for linear and isotropic materials are given in Eqs. (4, 5 and 6).

$$\varepsilon_x = \frac{1}{E}\left[\sigma_x - \vartheta\left(\sigma_y + \sigma_z\right)\right] \tag{4}$$

$$\varepsilon_y = \frac{1}{E}\left[\sigma_y - \vartheta\left(\sigma_z + \sigma_x\right)\right] \tag{5}$$

$$\varepsilon_z = \frac{1}{E}\left[\sigma_z - \vartheta\left(\sigma_x + \sigma_y\right)\right] \tag{6}$$

The changes between the lattice structures and unstressed condition samples are measured using XRD techniques. The changes in the structures are measured by using Bragg's law as given in Eq. 7. This equation is used to compute the reflection of X-rays from the weld surface.

$$n\lambda = 2dsin\theta \tag{7}$$

In the above equation, λ is the order of reflection. The surface strains are measured with diffraction technique, the RS ($\sigma_\varnothing$) is compute from the following Eq. (8).

$$\sigma_\varnothing = \frac{m}{d_0}\left(\frac{E}{1+v}\right) \tag{8}$$

where m = slope, of lattice space d against $sin^2\psi$ graph, d_0= Inter-planar lattice space in unstressed specimen.

Fig. 7 Welding setup with clamping

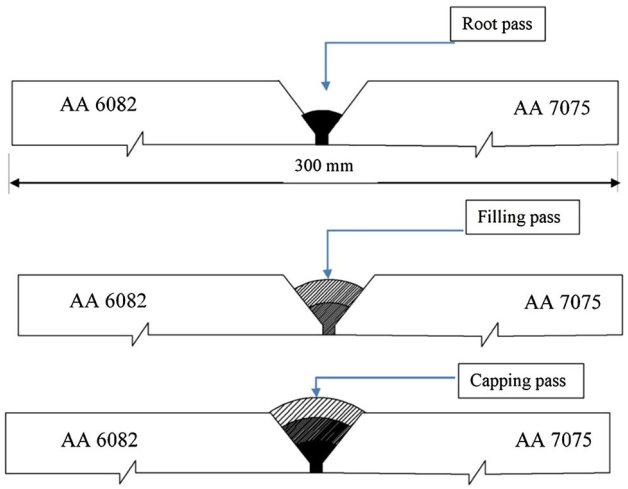

Fig. 8 Root, filling and capping passes for developing joint

4 Results and discussions

4.1 Simulation

The peaks during numerical simulation were predicted at time intervals of 10 s, 25 s and 44 s and are shown in Fig. 12. The peak temperatures at 10 s and 25 s was captured and were observed that 796 °C and 925 °C respectively. The temperature distribution was plotted from the data obtained after simulation as shown in Fig. 13. For the diagrammatic comparison of temperature gradients along transverse direction, combined temperature profiles were drawn. For pass-1, along the transverse direction, the maximum temperature observed was 738 °C. In pass-2, the peak temperature of 794 °C was predicted along transverse direction. Also, the high temperature of 532 °C and 564 °C was predicted at the AA7075 HAZ and AA6082 HAZ, respectively due to high thermal conductivity of base metal AA6082. Difference in temperatures was observed in the AA6082 HAZ and the AA7075 HAZ due differences in their thermal conductivities. The peak value 945 °C was observed pass-3 and similar kind of observation was observed in HAZ of both the metals. In all the passes, the higher temperature values were predicted at the 6082 HAZ. Weld puddle cools under the influence of conduction and convection heat transfer towards the base metal as the torch moves to the next position at each time increment. During welding, it has been observed that the number of improper temperature gradients were increasing with more passes and hence they have been restricted to three.

The thermal stresses were predicted in each pass and plots were shown in Fig. 14. In pass-1, the peak RS of 113.8 MPa was predicted at FZ whereas the RS value at HAZ of AA 6082 and AA7075 was predicted as 15.6 MPa (compressive) and 53.4 MPa (tensile) respectively. In pass-2, the high RS of 82.4 MPa was predicted at FZ whereas the stress value at HAZ of AA 6082 and AA7075 was predicted as 23.9 MPa

(compressive) and 8.6 MPa (tensile) respectively. In pass-3, the peak RS of 93.3 MPa (compressive) was predicted at FZ whereas the stress value at HAZ of AA 6082 and AA7075 was predicted as 5.7 MPa (compressive) and 4.6 MPa (tensile) respectively. From this plots, it is observed that non-uniform stress distributions was observed in pass-1 and pass-2. In pass-3, the stress distribution was uniform and well-balanced within the welded structures.

4.2 Experimentation

The temperature profiles along the transverse direction was analyzed by plotting a line in the opposite direction of welding. In thermal images as shown in Fig. 15, AA6082 is identified above the weld line and AA7075 below the weld line. The peak temperature at fusion zone is recorded as 847 °C, 879 °C, and 994 °C in passes-1, 2 and 3 correspondingly. A temperature difference was recorded from the image of AA6082 HAZ in comparison with AA7075 HAZ due to the variations in conductivities. The peak temperature of 693 °C and 604 °C was recorded at the HAZ of AA6082 and AA7075 HAZ, respectively. Similar kind of observations were observed in dissimilar welds of Inconel and AISI 316 due to the thermal differences [36]. The distribution along welding and towards base metal directions was recorded and plots are shown in Fig. 16. An incremental thermal cycles were observed when number of welding passes performed due to the transient conditions. From the temperature profiles along transverse direction, the peak temperature of 706 °C, 856 °C and 1012 °C was recorded in all passes.

The RS are measured using XRD technique and the peaks are shown in Fig. 17. On the weld surface of pass-1, compressive nature RS with a high value of 66 MPa was perceived (shown in Fig. 18). The RS across base metal direction in AA6082 was observed as 45 MPa and in AA7075 side it was measured as and 55 MPa. On the weld surface of pass-2, compressive natured RS with lower value of 28 MPa was perceived. The RS in AA6082 and AA7075 was measured as 36 MPa and 64 MPa, respectively. On the weld surface of pass-3 compressive nature RS with a higher value of 85 MPa was perceived. The RS in AA6082 and AA7075 is observed as -14 MPa and 12 MPa, respectively.

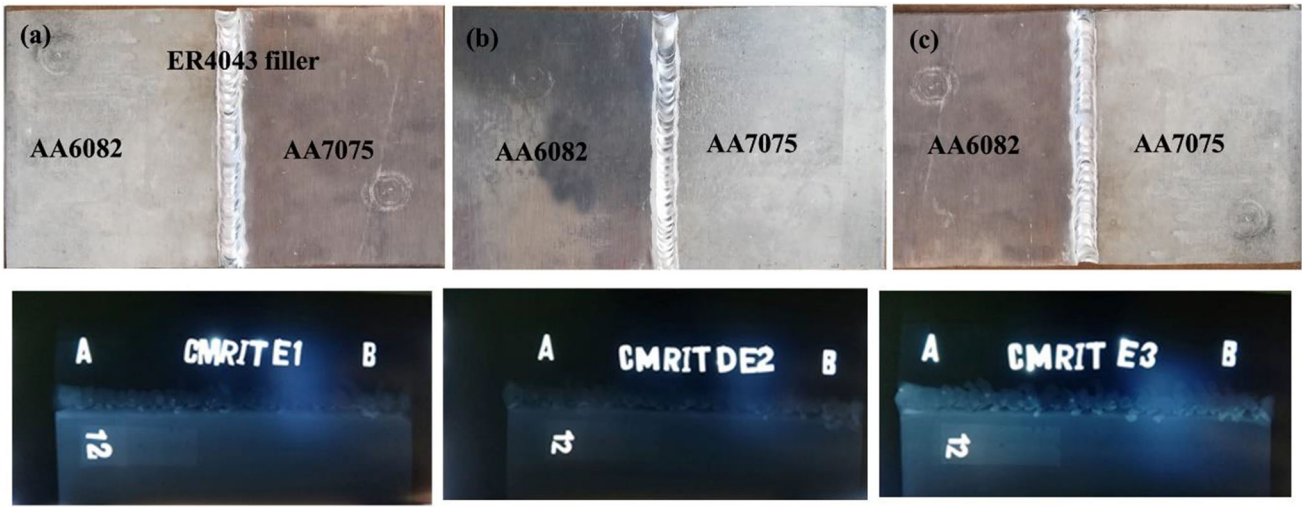

Fig. 9 Developed dissimilar welds of AA6082 and AA7075

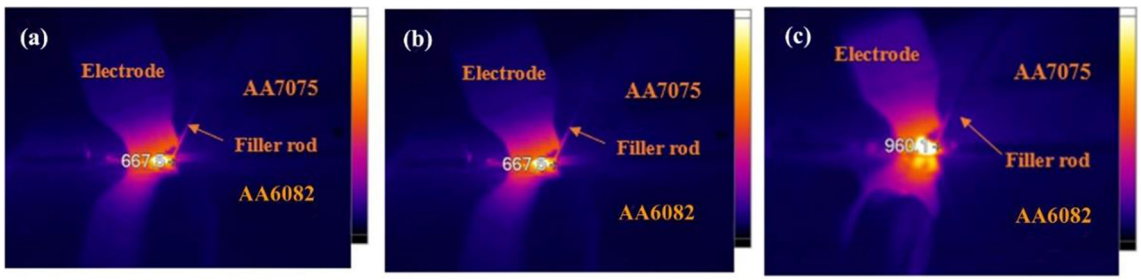

Fig. 10 IR images during welding in each pass

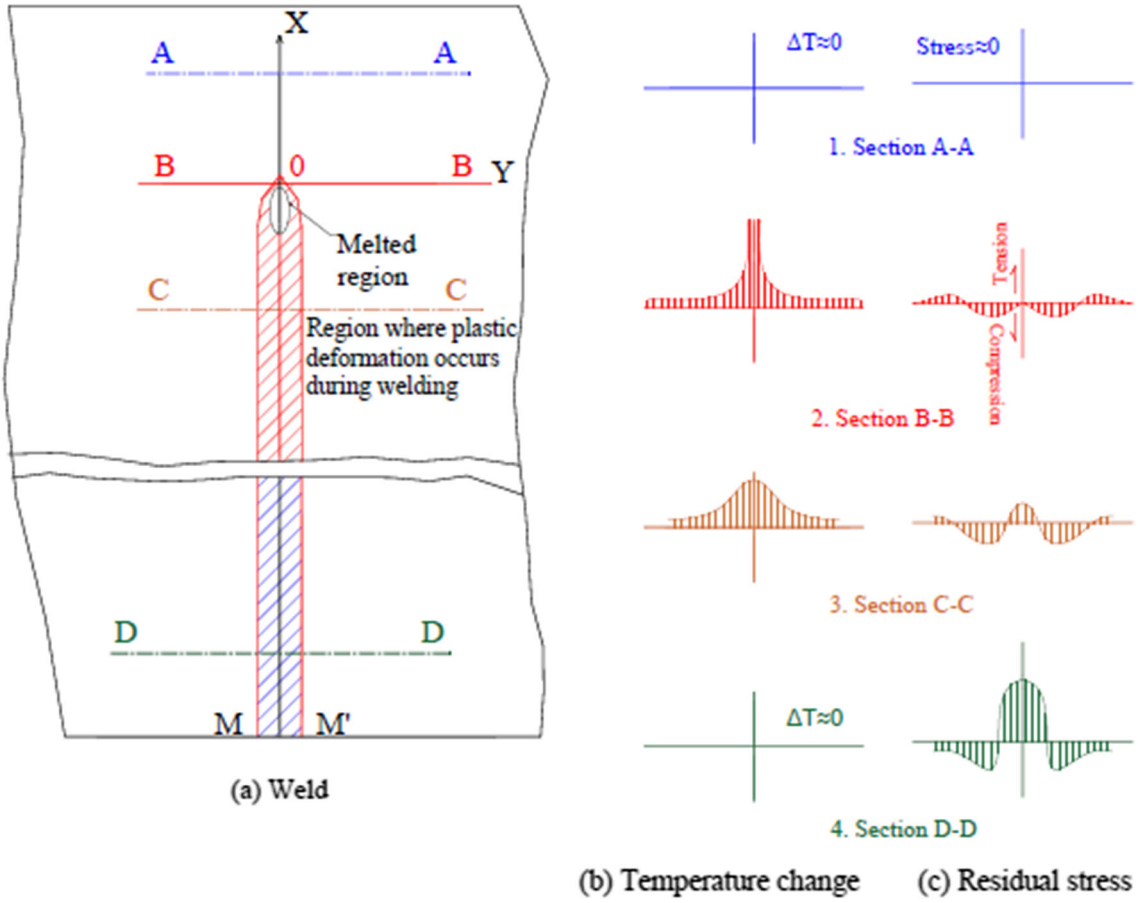

Fig. 11 Thermal stress formation during course of welding process

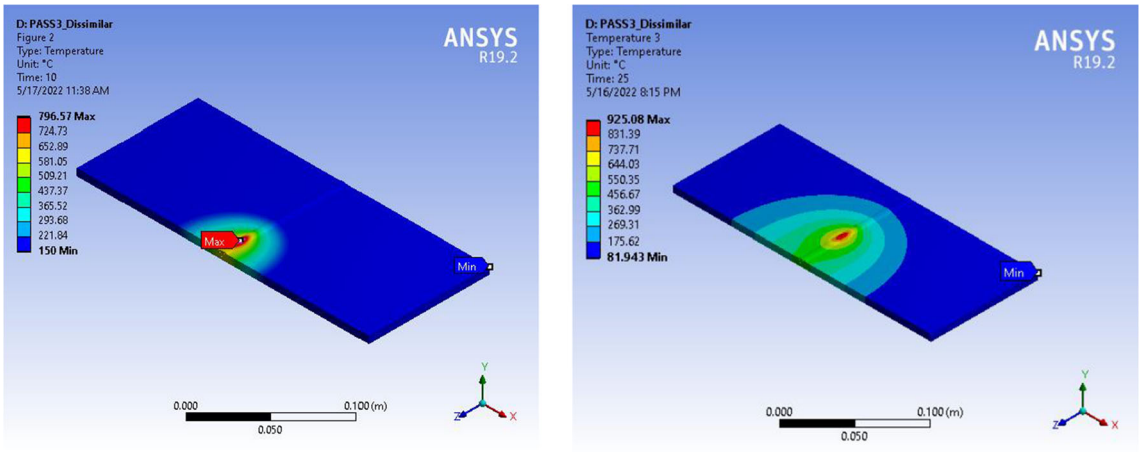

Fig. 12 Peak temperatures predicted in pass-3 at 10 s and 25 s

4.3 Validation of FE analysis

The higher temperature of 847 °C was recorded in pass-1 from IR thermography whereas, 738 °C was predicted in FE analysis. The peak temperature of 879 °C was recorded in pass-2 from IR thermography whereas, 794 °C was predicted in FE analysis. The peak temperature of 994 °C was recorded in pass-3 from IR thermography whereas, 945 °C was predicted in FE analysis. From the experimental and simulation analyses, the similar kind of peak and their distributions towards the base metals and transient thermal conditions were observed in both the analyses. The predicted simulation

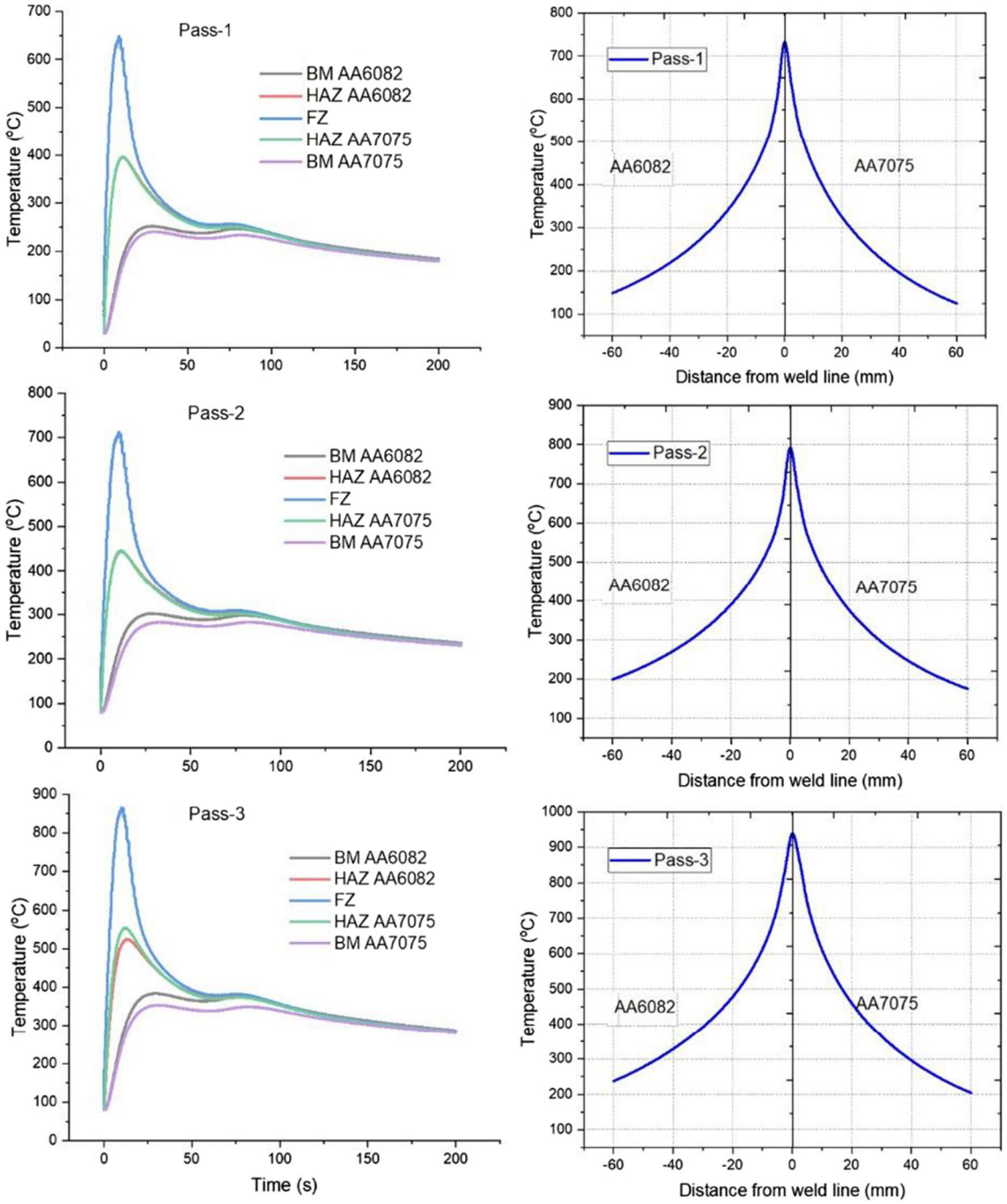

Fig. 13 Thermal cooling cycles and temperature distribution

results are very close to the experimentally recorded values with XRT technique. The predicted stress formation in the structures are validated with measured XRD data as shown in Fig. 17. The higher CRS are observed as 93.3 MPa and 85 MPa in FE analysis and experimentation results respectively. At the AA7075 HAZ, the TRS of 4.6 MPa and 12 MPa was perceived in ANSYS and results obtained from testing respectively. On surface of AA6082 HAZ, CRS of 5.7 MPa

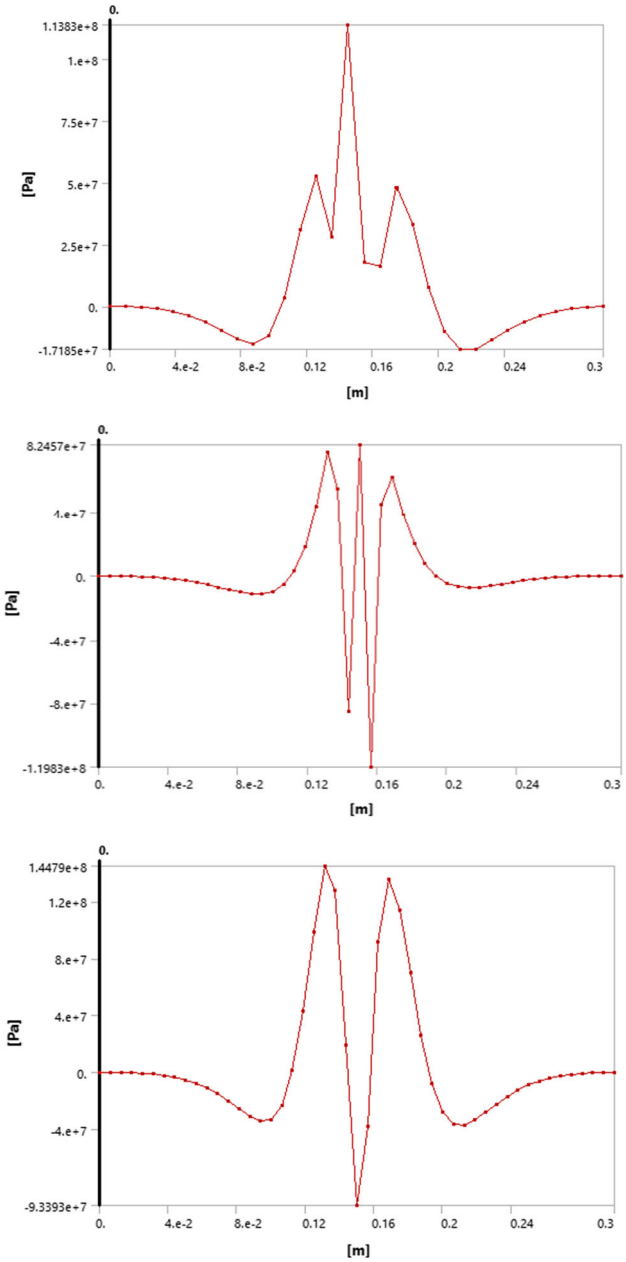

Fig. 14 Thermal stress distribution in each pass (Top side: pass-1, middle side: pass-2, and bottom side- pass-3)

and 14 MPa was perceived in FE and XRD results respectively. The experimentally measured data is found to be in line with FE analysis predicted data (Fig. 18).

5 Conclusions

This research work explores the prediction of temperature, distribution and heating and cooling cycles in AA6082 and AA 7075 welds in each welding pass. To validate the predicted data, experimental investigation was made to record peak temperatures and thermal distributions using IRT technique and measured residual stress formation using XRD methods. The following conclusions are mentioned from the numerical experimental investigations on thermal and structural fields of welded joints;

- The root, filling, and capping passes dissimilar welds of AA6082 and AA7075 were developed successfully using GTA welding process with ER4043 filler wire.
- The maximum temperature of 735 °C, 794 °C and 945 °C was predicted in three passes respectively. The thermal distribution towards the parent metal AA6082 is observed to be more than that of parent metal AA7075 because of its thermal properties at 550 °C. The transient thermal effects can be seen along the welding direction in all the passes during welding process.
- The maximum predicted residual stresses values in three passes respectively was observed as 113 MPa, 82 MPa and -93 MPa. The balanced thermal stresses were observed in final pass weldments and are within the yield limit only.
- The maximum temperature of 847 °C, 879 °C and 994 °C was observed in three passes respectively. Lower temperatures were captured at the AA7075 side than that of HAZ of AA6082 side. The peak value was 14.7% lower at HAZ of AA7075 than that of AA6082.
- The maximum observed residual stress values in three passes respectively were obtained as 66 MPa, 58 MPa and 45 MPa. Lower stresses at the HAZ of AA6082 are obtained in comparison to values at AA7075 HAZ due to accumulation of heat on AA7075 side.
- In final passes, weld zone has produced compressive residual stresses and the sign changed from compressive to tensile as moved towards base metals. The stresses were found to be self-balanced within the weld.
- The predicted thermal fields from FEA are in accordance with measured thermal fields from IR thermography. The deviation from the experimental results is less than 4.5%.

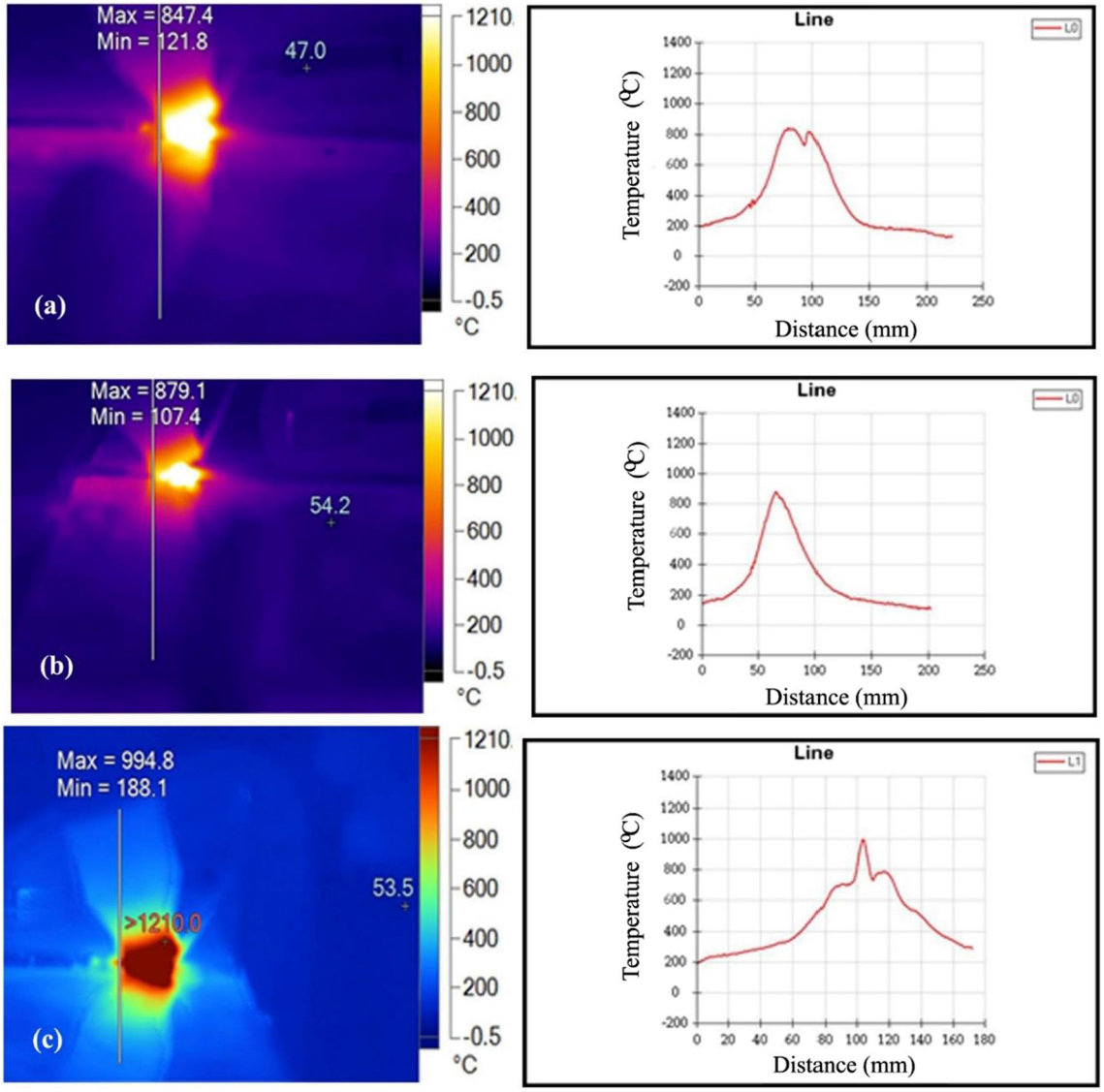

Fig. 15 Thermal cycles in each pass **a** pass-1, **b** pass-2 and **c** pass-3

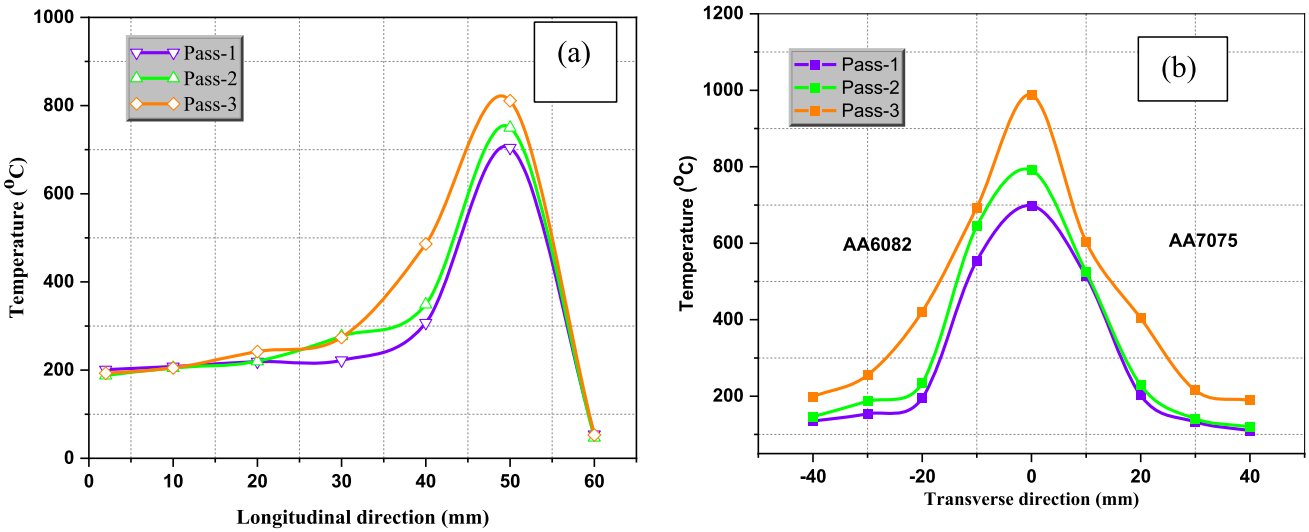

Fig. 16 Thermal cycles during weld process **a** longitudinal **b** transverse direction

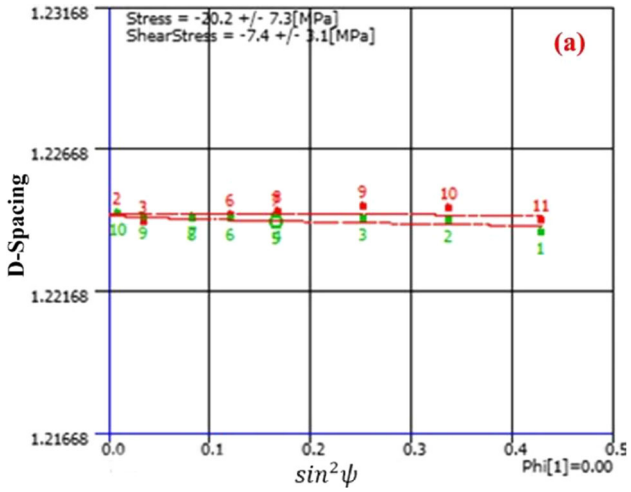

Fig. 17 XRD slope (D spacing vs $Sin^2\Psi$)

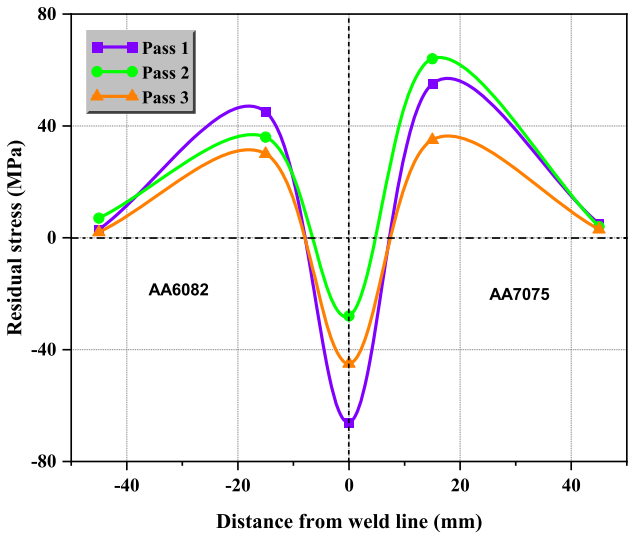

Fig. 18 RS formation in each pass

References

1. Sindo Kou, WELDING METALLURGY (SECOND EDITION) , John Wiley & Sons, Inc., Hoboken, New Jersey (2003).
2. Madani, T., Boukraa, M., Aissani, M., Chekifi, T., Ziadi, A., Zirari, M.: Experimental investigation and numerical analysis using Taguchi and ANOVA methods for underwater friction stir welding of aluminium alloy 2017 process improvement. Int. J. Press. Vessels Pip. (2023). https://doi.org/10.1016/j.ijpvp.2022.104879
3. Rishav Sen, S.P., Choudhury, R.K., Panda, A.: A comprehensive review on the feasibility study of metal inert gas welding. Mater. Today Proc. (2018). https://doi.org/10.1016/j.matpr.2018.06.104
4. Yelamasetti, B., Kumar, S., et al.: Effect of filler wires on weld strength of dissimilar pulse GTA Monel 400 and AISI 304 weldments. Mater. Today Proc. **19**, 246–250 (2019)
5. Chen, B.Q., Hashemzadeh, M., GuedesSoares, C.: Numerical and experimental studies on temperature and distortion patterns in butt-welded plates. Int. J. Adv. Manuf. Technol. **72**, 1121–1131 (2014). https://doi.org/10.1007/s00170-014-5740-8
6. Boukraa, M., Chekifi, T., Lebaal, N., et al.: Robust optimization of both dissolution time and heat affected zone over the friction stir welding process using SQP technique. Exp. Tech. **46**, 677–689 (2022). https://doi.org/10.1007/s40799-021-00515-8
7. DevendranathRamkumar, K., Arivazhagan, N., Narayanan, S.: Comparative assessment on microstructure and mechanical properties of continuous and pulse-current GTA welds of AISI 304 and Monel 400. Kov. Mater. **52**, 287–298 (2014). https://doi.org/10.4149/km-2014-5-287
8. Yelamasetti, B., Manikyam, S., Saxena, K.K.: Multi-response Taguchi grey relational analysis of mechanical properties and weld bead dimensions of dissimilar joint of AA6082 and AA7075. Adv. Mater. Process. Technol. **8**, 1474–1484 (2022)
9. Boukraa, M., Chekifi, T., Lebaal, N.: Friction stir welding of aluminum using a multi-objective optimization approach based on both Taguchi method and grey relational analysis. Exp. Tech. **47**, 603–617 (2023). https://doi.org/10.1007/s40799-022-00573-6
10. Chekifi, T., Boukraa, M.: Solar still productivity improvement using nanofluids: a comprehensive review. Int. J. Ambient Energy **44**, 1396 (2023). https://doi.org/10.1080/01430750.2023.2174185
11. Satyanarayana, I., Rajyalaxmi, N.: Thermal analysis of ceramic coated steel alloy piston used in diesel engine using FEM. Int. J. Innov. Sci. Eng. Technol. **3**, 245–250 (2016)
12. Balram, Y., Rajyalakshmi, G.: Thermal fields and residual stresses analysis in TIG weldments of SS 316 and Monel 400 by numerical simulation and experimentation. Mater. Res. Express (2019). https://doi.org/10.1088/2053-1591/ab23cf
13. Karunakaran, N.: Effect of pulsed current on temperature distribution and characteristics of GTA welded magnesium alloy. IOSR J. Mech. Civ. Eng. (2013). https://doi.org/10.9790/1684-0460108
14. Vasudevan, M., Chandrasekhar, M.N., Maduraimuthu, M.V., et al.: Real-time monitoring of weld pool during GTAW using infrared thermography and analysis of infra-red thermal images. Weld. World **55**, 83–89 (2011). https://doi.org/10.1007/BF03321311
15. Yelamasetti, B., Ramana, G.V., Manikyam, S., Vardhan, T.V.: Thermal field and residual stress analyses of similar and dissimilar weldments joined by constant and pulsed current TIG welding techniques. Adv. Mater. Process. Technol. (2021). https://doi.org/10.1080/2374068X.2021.1959114
16. Vemanaboina, H., Janardhana Raju, G., Sreenivas, B.: Temperature field and residual stress of Butt welding for IN plate. Int. J. Eng. Technol. (2018). https://doi.org/10.14419/ijet.v7i4.10.20713
17. Turan, M.E., Aydin, F., Sun, Y., Cetin, M.: Residual stress measurement by strain gauge and X-ray diffraction method in different shaped rails. Eng. Fail. Anal. **96**, 525–529 (2019)
18. Withers, P.J., Bhadeshia, H.K.D.H.: Residual stress. Part 1: measurement techniques. Mater Sci Technol **17**, 355–365 (2001). https://doi.org/10.1179/026708301101509980
19. Chang, P.-H., Teng, T.-L.: Numerical and experimental investigations on the residual stresses of the butt-welded joints. Comput. Mater. Sci. (2004). https://doi.org/10.1016/j.commatsci.2003.12.005
20. Yadav, A.K., Agrawal, M.K., Saxena, K.K., et al.: Numerical simulation and experimental residual stress analyses of dissimilar GTA weldments of AA 5083 and AA 6082. Int. J. Interact. Des. Manuf. (2023). https://doi.org/10.1007/s12008-023-01216-9
21. Javadi, Y., Smith, M.C., Abburi Venkata, K., et al.: Residual stress measurement round robin on an electron beam welded joint between austenitic stainless steel 316L(N) and ferritic steel P91. Int. J. Press. Vessel Pip. **154**, 41–57 (2017). https://doi.org/10.1016/j.ijpvp.2017.06.002
22. Zhou, H., Zhang, Q., Yi, B., Wang, J.: Hardness prediction based on microstructure evolution and residual stress evaluation during high tensile thick plate butt welding. Int. J. Nav. Archit. Ocean Eng. **12**, 146–156 (2020). https://doi.org/10.1016/j.ijnaoe.2019.09.004

23. Sun, J., Zhu, J., Xia, L., Deng, D.: Numerical simulation of welding residual stress and deformation induced by electro slag welding. Hanjie Xuebao Trans. China Weld. Inst. **37**, 23 (2016)
24. Deng, D., Murakawa, H., Liang, W.: Numerical simulation of welding distortion in large structures. Comput. Methods Appl. Mech. Eng. **196**, 4613–4627 (2007). https://doi.org/10.1016/j.cma.2007.05.023
25. Venkatkumar, D., Ravindran, D.: 3D finite element simulation of temperature distribution, residual stress and distortion on 304 stainless steel plates using GTA welding. J. Mech. Sci. Technol. **30**, 67–76 (2016). https://doi.org/10.1007/s12206-015-1208-5
26. Vemanaboina, H., Edison, G., Akella, S., Kumar Buddu, R.: Thermal Analysis simulation for laser Butt welding of Inconel625 using FEA. Int. J. Eng. Technol. **7**, 85 (2018). https://doi.org/10.14419/ijet.v7i4.10.20711
27. Yelamasetti, B., Manikyam, S., Ravindrakumar, Saxena, K.K.: Finite element simulation for predicting temperature and residual stresses distribution developed in dissimilar welds of Monel 400 and AISI 309L. Adv. Mater. Process. Technol. **8**, 1206–1216 (2022)
28. Bajpei, T., Chelladurai, H., Ansari, M.Z.: Numerical investigation of transient temperature and residual stresses in thin dissimilar aluminium alloy plates. Procedia Manuf. **5**, 558–567 (2016). https://doi.org/10.1016/j.promfg.2016.08.046
29. Bajpei, T., Chelladurai, H., Ansari, M.Z.: Mitigation of residual stresses and distortions in thin aluminium alloy GMAW plates using different heat sink models. J. Manuf. Process. **22**, 199–210 (2016). https://doi.org/10.1016/j.jmapro.2016.03.011
30. Yegaie, Y.S., Kermanpur, A., Shamanian, M.: Numerical simulation and experimental investigation of temperature and residual stresses in GTAW with a heat sink process of Monel 400 plates. J. Mater. Process. Technol **210**, 1690–1701 (2010). https://doi.org/10.1016/j.jmatprotec.2010.05.017
31. Lu, Y., Zhu, S., Zhao, Z., et al.: Numerical simulation of residual stresses in aluminum alloy welded joints. J. Manuf. Process. **50**, 380–393 (2020). https://doi.org/10.1016/j.jmapro.2019.12.056
32. Chen, J., Salvati, E., Uzun, F., et al.: An experimental and numerical analysis of residual stresses in a TIG weldment of a single crystal nickel-base superalloy. J. Manuf. Process. **53**, 190–200 (2020). https://doi.org/10.1016/j.jmapro.2020.02.007
33. Zubairuddin, M., Albert, S.K., Vasudevan, M., et al.: Finite element simulation of weld bead geometry and temperature distribution during GTA welding of modified 9Cr-1Mo steel and experimental validation. J. Manuf. Sci. Prod. **14**, 195–207 (2014). https://doi.org/10.1515/jmsp-2014-0006
34. BalramYelamasetti, M., Kumar, D., Saxena, K.K.: Experimental investigation on temperature profiles and residual stresses in GTAW dissimilar weldments of AA5052 and AA7075. Adv. Mater. Process. Technol. **8**, 352–365 (2022)
35. Goldak, J., Chakravarti, A., Bibby, M.: A new finite element model for welding heat sources. Metall. Trans. B **15**, 299–305 (1984). https://doi.org/10.1007/BF02667333
36. Yelamasetti, B., Ramana, G.V., Sanke, N., Gupta, N.: Numerical and experimental residual stress analysis of dissimilar metals of Inconel 718 and AISI 316 developed in GTAW process. Int. J. Interact. Des. Manuf. (2022). https://doi.org/10.1007/s12008-022-00932-y